ЖЭТФ, 2014, том 145, вып. 2, стр. 306–319

EFFECT OF Eu DOPING AND PARTIAL OXYGEN ISOTOPE SUBSTITUTION ON MAGNETIC PHASE TRANSITIONS IN $(Pr_{1-y}Eu_y)_{0.7}Ca_{0.3}CoO_3$ COBALTITES

N. A. Babushkina [a*], ***A. N. Taldenkov*** [a], ***S. V. Streltsov*** [b,c], ***A. V. Kalinov*** [d], ***T. G. Kuzmova*** [e], ***A. A. Kamenev*** [e], ***A. R. Kaul*** [e], ***D. I. Khomskii*** [f], ***K. I. Kugel*** [g]

[a] *National Research Center "Kurchatov Institute" 123182, Moscow, Russia*

[b] *Institute of Metal Physics, Ural Branch, Russian Academy of Sciences 620990, Ekaterinburg, Russia*

[c] *Ural Federal University 620002, Ekaterinburg, Russia*

[d] *All-Russian Electrical Engineering Institute 111250, Moscow, Russia*

[e] *Department of Chemistry, Moscow State University 119991, Moscow, Russia*

[f] *II. Physikalisches Institut, Universität zu Köln 50937, Köln, Germany*

[g] *Institute for Theoretical and Applied Electrodynamics, Russian Academy of Sciences 125412, Moscow, Russia*

Received May 22, 2013

We study experimentally and theoretically the effect of Eu doping and partial oxygen isotope substitution on the transport and magnetic characteristics and spin-state transitions in $(Pr_{1-y}Eu_y)_{0.7}Ca_{0.3}CoO_3$ cobaltites. The Eu doping level y is chosen in the range of the phase diagram near the crossover between the ferromagnetic and spin-state transitions ($0.10 < y < 0.20$). We prepared a series of samples with different degrees of enrichment by the heavy oxygen isotope ^{18}O, namely, with 90 %, 67 %, 43 %, 17 %, and 0 % of ^{18}O. Based on the measurements of the ac magnetic susceptibility $\chi(T)$ and electrical resistivity $\rho(T)$, we analyze the evolution of the sample properties with the change of the Eu and ^{18}O content. It is demonstrated that the effect of increasing the ^{18}O content on the system is similar to that of increasing the Eu content. The band structure calculations of the energy gap between t_{2g} and e_g bands including the renormalization of this gap due to the electron–phonon interaction reveals the physical mechanisms underlying this similarity.

DOI: 10.7868/S0044451014020114

1. INTRODUCTION

Most magnetic oxides are characterized by a strong interplay of electron, lattice, and spin degrees of freedom giving rise to multiple phase transitions and different types of ordering. The phase transitions are often accompanied by the formation of different inhomogeneous states. In such a situation, the oxygen isotope substitution provides a unique tool for investigating inhomogeneous states in magnetic oxides, which allows studying the evolution of their properties in a wide range of the phase diagram. Sometimes, especially if a system is close to the crossover between different states (usually leading to phase separation), the isotope substitution can lead to significant changes in the ground state of the system [1].

*E-mail: babushkina_NA@nrcki.ru

A good example of such phenomena is provided by cobaltites. These perovskite cobalt oxides have attracted special interest owing to the possibility of the spin-state transitions (SST) for Co ions induced by temperature or doping [2–8] and the related phase separation phenomena [9–16]. The effect of $^{16}O \rightarrow ^{18}O$ isotope substitution on the properties of $(Pr_{1-y}Eu_y)_{0.7}Ca_{0.3}CoO_3$ cobaltites ($0.12 < y < 0.26$) was studied previously in our paper [17]. It was found that with increasing the Eu content, the ground state of the compound changes from a "nearly metallic" ferromagnet (ferromagnetic metallic clusters embedded into an insulating host) to a "weakly magnetic insulator" at $y < y_{cr} \approx 0.18$, regardless of the isotope content. A pronounced SST was observed in the insulating phase (in samples with $y > y_{cr}$), whereas in the nearly metallic phase (at $y < y_{cr}$), the magnetic properties were quite different, without any indications of a temperature-induced SST. Using the magnetic, electrical, and thermal data, we constructed the phase diagram for this material. The characteristic feature of this phase diagram is a broad crossover range near y_{cr} corresponding to a competition of the phases mentioned above. The $^{16}O \rightarrow ^{18}O$ substitution gives rise to an increase in the SST temperature T_{SS} and to a slight decrease in the ferromagnetic (FM) transition temperature T_{FM}.

However, a number of problems important for understanding the physics of systems with spin-state transitions have not been considered in the study reported in Ref. [17]. The most important question is the relation between the changes caused by varying the composition (increase of the concentration y of the smaller rare-earth ions Eu) and by isotope substitution, and the physical mechanism underlying these changes. From the phase diagram obtained in Ref. [17] and in this paper, we see that there exists some correlation between these changes, but the situation is not so simple: in the right part of the phase diagram, the SST temperature increases both with the increase in the Eu content y and with the increase in the isotope mass (in passing from ^{16}O to ^{18}O). At the same time, in the left part of this phase diagram, the effect of increasing the Eu content and of increasing the oxygen mass on the phase transition (which is then the transition to a nearly ferromagnetic state) is just the opposite: an increase in the Eu content leads to a decrease in T_{FM}, but the increase in oxygen mass, to the increase in T_{FM}.

Another important open question concerns the behavior of separate phases in the regime of phase separation. There are many different correlated systems in which phase separation was detected in some range of compositions, temperatures, external fields, etc. Typically, the measured transition temperatures in this case changes, e. g., with doping. But it often remains unclear whether this change is the effect occurring in separate regions of different phases or is just the result of averaging over the inhomogeneous system. To answer these questions, we now carried out a detailed study of the behavior of $(PrEu)CoO_3$ using the possibility of fine tuning the properties of the system by partial isotope substitution. This partial substitution plays in effect the role similar to that of doping, external pressure, etc. The obtained results establish the possibility of "rescaling" the changes in the system with doping and with isotope substitution and allow us to clarify the questions formulated above.

As regards the second question formulated above, just the possibility of fine tuning the properties of the system inside the region of phase separation, provided by partial isotope substitution, allows studying the behavior of different phases within this phase-separated regime individually which would be very difficult to achieve by other means. Our results obtained in this way demonstrate that not only the average critical temperatures change with doping and with isotope substitution but also "individual" transition temperatures (the ferromagnetic transition temperature in more metallic regions and the SST temperature in more insulating parts of the sample) do change with the chemical and isotope composition.

As regards the main, first question formulated above, about the mechanisms governing the change of properties of the system with chemical and isotope composition, the experimental findings reported in this paper allow us to formulate a realistic theoretical model clarifying the mechanisms underlying the pronounced isotope effects in cobaltites exhibiting SSTs. The theoretical analysis demonstrates that the main factor is the change of the effective bandwidth with the change of both chemical and isotope composition. The opposite trends in two parts of the phase diagram mentioned above find a natural explanation in this picture.

To analyze the effects of partial oxygen isotope substitution for doped cobaltites in the crossover region of the phase diagram, we have prepared a series of oxide materials with a nearly continuous tuning of their characteristics. This allows tracing the evolution of the relative content of different phases as a function of the ratio $^{18}O/^{16}O$ of the contents of oxygen isotopes. We note that there were only a few investigations of this kind, one of which we undertook earlier for $(La_{1-y}Pr_y)_{0.7}Ca_{0.3}MnO_3$ manganites [18]. Here, the pronounced isotope effect manifesting itself in

$(Pr_{1-y}Eu_y)_{0.7}Ca_{0.3}CoO_3$ cobaltites indeed provides us with a unique possibility to address the problems discussed above through the use of partial oxygen isotope substitution.

2. EXPERIMENTAL

Polycrystalline $(Pr_{1-y}Eu_y)_{0.7}Ca_{0.3}CoO_3$ samples were prepared by the chemical homogenization ("paper synthesis") method [19] through the use of the following operations. At first, nonconcentrated water solutions of metal nitrates $Pr(NO_3)_3$, $Eu(NO_3)_3$, $Ca(NO_3)_2$, and $Co(NO_3)_2$ of 99.95 % purity were prepared. The exact concentration of dissolved chemicals was established by gravimetric titration and, in the case of Co-based solution, by means of potentiometric titration. The weighted amounts of metal nitrate solutions were mixed in the stoichiometric ratio and the calculated mixture of nitrates was dropped onto ash-free paper filters. The filters were dried out at about 80 °C and the procedure of the solution dropping was performed repeatedly. Then, the filters were burned out and the remaining ash was thoroughly ground. It was annealed at 800 °C for 2 h to remove carbon. The powder obtained was pressed into the pellets and sintered at 1000 °C in the oxygen atmosphere for 100 h. Finally, the samples were slowly cooled to room temperature by switching off the furnace.

Samples were analyzed at room temperature by the powder X-ray diffraction using Cu K_α radiation. All detectable peaks were indexed by the *Pnma* space group. According to the X-ray diffraction patterns, all $(Pr_{1-y}Eu_y)_{0.7}Ca_{0.3}CoO_3$ samples were obtained as single-phase polycrystalline materials.

We prepared a series of ceramic cobaltite samples with the degrees of enrichment by ^{18}O equal to 90 %, 67 %, 43 %, 17 %, and 0 %. These values were determined by the changes in the sample mass in the course of the isotope exchange and by the mass spectrometry of the residual gas in the oxygen exchange contour. The samples were annealed in the appropriate ^{16}O–^{18}O gas mixture at 950 °C during 48 h at a total pressure of 1 bar. The similarity of the oxygen isotope composition in the sample to that in the gas medium indicated that a thermodynamic equilibrium was achieved during annealing and, hence, the difference in the diffusion rates of the oxygen isotopes did not significantly affect the results of the investigation. We also note that the mass of a sample annealed in $^{16}O_2$ remained unchanged within the experimental error during the prolonged heat treatment. Therefore, we can conclude that the annealing procedure does not change the oxygen stoichiometry in the compounds under study.

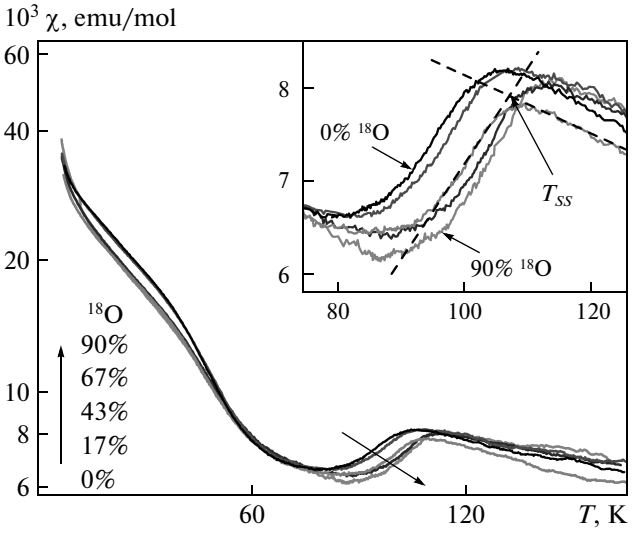

Fig. 1. Temperature dependence of the magnetic susceptibility for $(Pr_{1-y}Eu_y)_{0.7}Ca_{0.3}CoO_3$ with $y = 0.2$. The range in the vicinity of the SST is shown in the inset in a larger scale. The dashed straight lines illustrate determining the value of T_{SS}

The Eu doping of these samples was chosen to be near and at both sides of the crossover doping level y_{cr}: a composition with the high Eu content exhibiting the SST, a low-Eu composition corresponding to the nearly ferromagnetic state, and the sample at the phase crossover, where both T_{SS} and T_{FM} were observed.

We note that the set of samples described above was specially prepared for the present study. It turned out that the data obtained for these samples differ somehow from those reported in Ref. [17] (samples of set 1). In particular, the values of the transition temperatures between phases are different for these two sets of samples. We thoroughly analyzed the possible causes of this difference. The samples of both sets prepared by the same technique do not differ by X-ray diffraction data, have the same oxygen stoichiometry, but the calcium content in set 1 appeared to be lower than that corresponding to the nominal composition. At the same time, the samples of set 2 correspond with a high accuracy to the chemical formula $(Pr_{1-y}Eu_y)_{0.7}Ca_{0.3}CoO_3$. As is discussed below, this leads to some general shift of the phase diagram toward larger values of the average ionic radius $\langle r_A \rangle$ (i. e., to the lower Eu content). Nevertheless, the general form of the phase diagram remains the same.

For all samples, we measured the temperature dependence of the real $\chi'(T)$ and imaginary $\chi''(T)$ parts

of the ac magnetic susceptibility and electrical resistivity $\rho(T)$. The resistivity measurements discussed below were taken on cooling the samples. The measurements of the ac magnetic susceptibility $\chi(T)$ were performed in an ac magnetic field with the frequency 667 Hz and an amplitude of about 5 Oe in the dc magnetic field of Earth. Based on these measurements, we were able to analyze the evolution of the sample properties with the change in the Eu and ^{18}O content. To achieve a better reliability, the isotope shifts $\Delta T_{FM} = T_{FM}(M) - T_{FM}(^{16}\mathrm{O})$ and $\Delta T_{SS} = T_{SS}(M) - T_{SS}(^{16}\mathrm{O})$ (where M is the average atomic mass of oxygen isotopes) were determined based on the susceptibility data obtained both on cooling and on heating. Within the experimental error, we did not observe a temperature hysteresis in the vicinity of the transition to the ferromagnetic phase, whereas near the SST, the hysteresis did not exceed 1 K. In the figures in what follows, we present the $\chi(T)$ plots corresponding to the heating of the samples. The T_{FM} transition temperatures were determined from the minimum of the logarithmic temperature derivative of the susceptibility. The T_{SS} transition temperatures were determined by linear approximation as demonstrated in Fig. 1. Although the critical temperatures depend on the chosen method with which they are determined, the isotopic shift is nearly insensitive to the choice of the determination procedure. The resistivity of the samples was measured by the conventional four-probe technique in the temperature range from 4.2 K to 300 K. The value of the metal–insulator transition temperature T_{MI} can be determined from the logarithmic derivative of $R(T)$ (see the inset of Fig. 2).

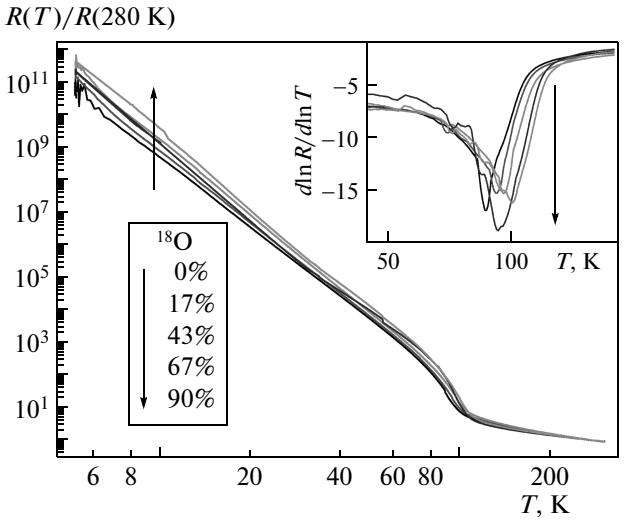

Fig. 2. Temperature dependence of the electrical resistivity for $(Pr_{1-y}Eu_y)_{0.7}Ca_{0.3}CoO_3$ with $y = 0.2$. The inset shows the behavior of the logarithmic derivative of $R(T)$ used to determine the values of T_{MI}

3. EXPERIMENTAL RESULTS

1. For the samples with $y > y_{cr}$ (the Eu content $y = 0.20$), the material corresponds to a "weakly magnetic insulator", in the notation used in Ref. [17]. The $\chi'(T)$ curves give clear indications of an SST at T_{SS} manifesting itself as a peak in $\chi'(T)$ (see Fig. 1). We see that T_{SS} increases with the ^{18}O content. The high-temperature phase is a paramagnet and a relatively good conductor (see Fig. 2).

The low-spin (LS) insulating phase is dominant below the crossover temperature of about 100 K. The increase in χ' at low temperatures is most probably caused by an incomplete transition, after which there may remain small magnetic (and presumably more conducting) clusters immersed into the LS state bulk insulator. As a result of this crossover to an LS state, the electrical resistance R increases by 10–12 orders of magnitude, which can be treated as a metal–insulator (MI) transition (see Fig. 2). In these compounds, the metal–insulator transition is accompanied (or caused) by the SST. We note that the studies of the oxygen isotope effect are performed in most cases using low-density ceramic samples with open porosity. This gives rise to the granularity effects related to the existence of thin spacers at the grain boundaries with the properties somehow different from those of the grains themselves. In the magnetic oxides under study, the phase separation coming from the competition between different kinds of the exchange interaction also manifests itself.

All these factors lead to significant changes in the temperature dependence of electrical resistivity, such that the temperature derivative of R remains negative for the compositions under study. Nevertheless, the characteristic features of $R(T)$, which are observed in the vicinity of the SST and are suppressed in the composition range corresponding to ferromagnetism, allow arguing that we see a manifestation of the metal–insulator transition in one of the phases.

The ^{18}O content does not produce a significant effect on $R(T)/R(280\ \mathrm{K})$ at low T, although $R(T)/R(280\ \mathrm{K})$ is slightly larger in the samples with heavy oxygen. The mass dependence of T_{MI} correlates well with the isotopic shift of T_{SS} (see Fig. 3). According to the calculation of the isotopic constant $T \sim M^{-\alpha}$ (where M is the averaged oxygen mass),

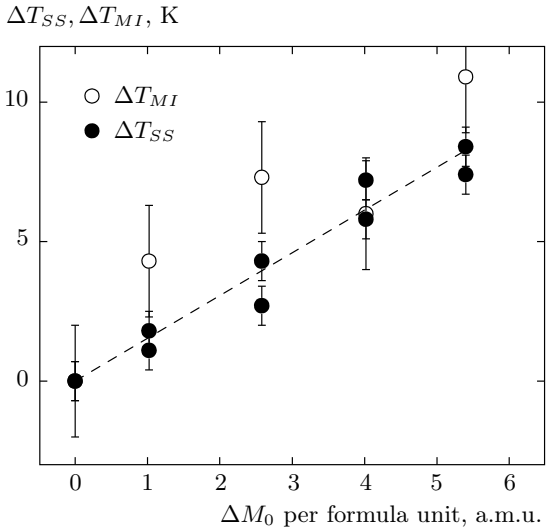

Fig. 3. Isotopic shift of the characteristic temperatures of the spin-state T_{SS} and metal–insulator T_{MI} transitions at the $^{16}O \rightarrow {}^{18}O$ substitution for the sample with $y = 0.2$. The values of T_{SS} were determined both on cooling and on heating the samples (two closed circles at each isotope content)

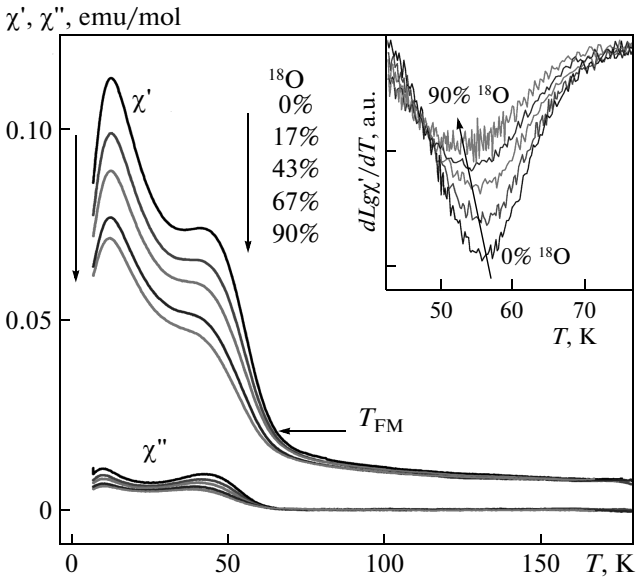

Fig. 4. Temperature dependence of the magnetic susceptibility for $(Pr_{1-y}Eu_y)_{0.7}Ca_{0.3}CoO_3$ with $y = 0.14$. The inset illustrates the behavior of the logarithmic derivative of $\chi'(T)$ in the vicinity of T_{FM} used to determine the values of T_{FM}

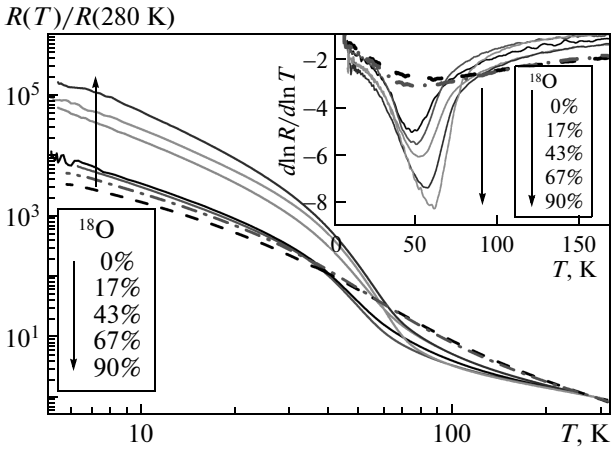

Fig. 5. Temperature dependence of the electrical resistivity for $(Pr_{1-y}Eu_y)_{0.7}Ca_{0.3}CoO_3$ with $y = 0.14$ (solid line) and $y = 0.1$ with ^{16}O (dashed line) and ^{18}O (dash-doted line). The inset illustrates the behavior of the logarithmic derivative of $R(T)$ used to determine the values of T_{FM}

$\alpha = -d\ln T/d\ln M = -(\Delta T/\Delta M)(M/T)$, we have the value α_{SS} and $\alpha_{MI} = -(0.66 \pm 0.07)$. Increasing the oxygen mass promotes the development of the LS state.

2. The most important results are obtained for the samples with the Eu content $y \sim y_{cr}$ ($y = 0.14$, 0.16). They correspond to a wide concentration range of phase separation.

For the sample with $y = 0.14$, we observe a feature in $\chi'(T)$ curves corresponding to a steep increase of the magnetization on cooling at 60–70 K (see Fig. 4). This behavior is caused by the FM phase arising in these samples. In addition, in the temperature dependence of resistivity, we see a steep increase in resistivity characteristic of the metal–insulator transition similar to that observed for the samples with $y = 0.2$ (see Fig. 5). The transition temperature corresponds to the minimum of the logarithmic derivative of the resistivity (see the inset in Fig. 5). This means that here we also deal with the change in the relative content of metallic and insulating phases, suggesting the existence of regions corresponding to the LS insulating state and the correlation between the MI and SS transitions. At the same time, we do not observe any clear indications of the SST in the temperature dependence of the magnetic susceptibility. For example, the samples with $y = 0.14$ turn out to be at the boundary of the phase separation range. Increasing the oxygen mass favors the LS state as well as suppression of the FM phase and of the metallization.

The values of the isotopic constant calculated for the MI and FM transitions in this sample are $\alpha_{MI} = -(2.1 \pm 0.1)$ and $\alpha_{FM} = (0.5 \pm 0.05)$. For this sample,

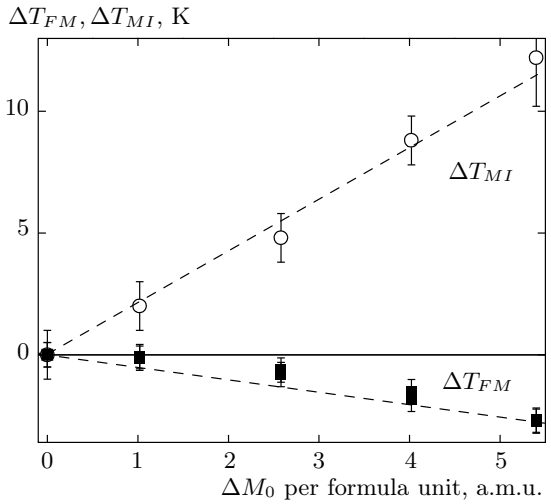

Fig. 6. Isotopic shift of the characteristic temperatures of the spin-state T_{SS}, metal–insulator T_{MI}, and ferromagnetic T_{FM} transitions for the sample with $y = 0.14$. The spin-state transition temperature T_{SS} actually coincides with T_{MI}. The values of T_{FM} were determined both on cooling and heating the samples (two nealy coinciding closed squares at each isotope content)

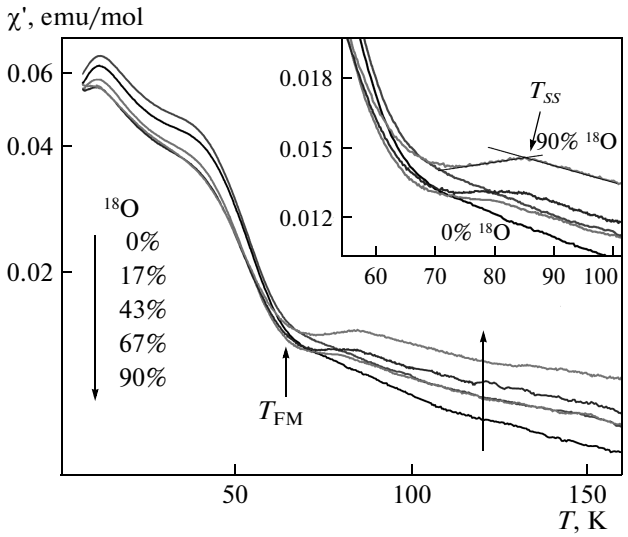

Fig. 7. Temperature dependence of the magnetic susceptibility for $(Pr_{1-y}Eu_y)_{0.7}Ca_{0.3}CoO_3$ with $y = 0.16$. The inset illustrates the behavior of $\chi'(T)$ in a larger scale. The straight lines in the inset illustrate determining the value of T_{SS} used to determine the values of T_{MI}

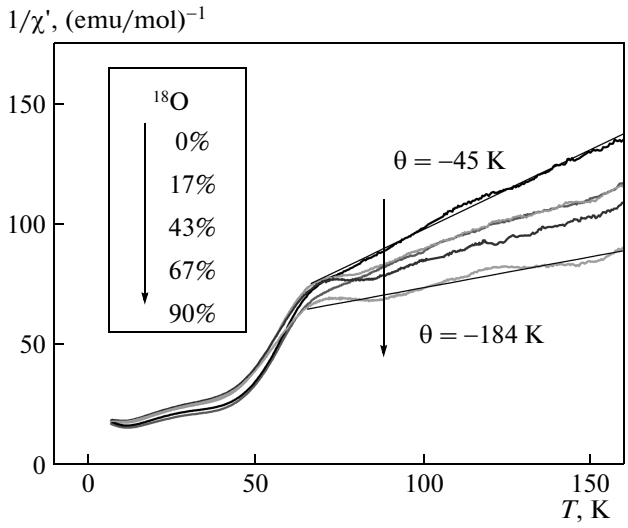

Fig. 8. Temperature dependence of the inverse magnetic susceptibility for $(Pr_{1-y}Eu_y)_{0.7}Ca_{0.3}CoO_3$ with $y = 0.16$

the isotope shifts of the characteristic transition temperatures are illustrated in Fig. 6.

For the samples with $y = 0.16$, the effect of the partial oxygen isotope substitution by ^{18}O manifests itself even clearly. Here, we observed the features characteristic of both FM and SS transitions. On the one hand, the temperature dependence of χ' exhibits a steep increase at 60–70 K similar to that in the $y = 0.14$ sample indicating the existence of the FM transition. On the other hand, in $\chi'(T)$, we observed a clearly pronounced peak, which can be attributed to the SST at T_{SS} (Fig. 7). The $\chi'(T)$ curves also demonstrate that the transition to the LS state gradually disappears as the oxygen mass decreases. In samples with a low ^{18}O content ($< 17\,\%$), this transition is hardly seen due to the gradual transformation from the LS to FM state when the oxygen mass decreases. The curves for samples with 17 % and 43 % of ^{18}O corresponding to the crossover range between different phase states nearly coincide. We also note that for $y = 0.16$ (as well as in the samples with $y = 0.14$), the temperature T_{FM} decreases as the average mass of oxygen increases.

In addition, the Curie–Weiss temperature θ in the formulas for the inverse magnetic susceptibility $\chi^{-1}(T)$ considerably decreases with the increase in the average mass of oxygen isotopes (see Fig. 8). For the samples with the largest oxygen mass, we have $\theta = -184$ K, whereas for the samples with ^{16}O, $\theta = -45$ K. This phenomenon may be related to the transition from the antiferromagnetic interaction to the ferromagnetic one. We note that Fig. 4 demonstrates that χ'' is nearly zero

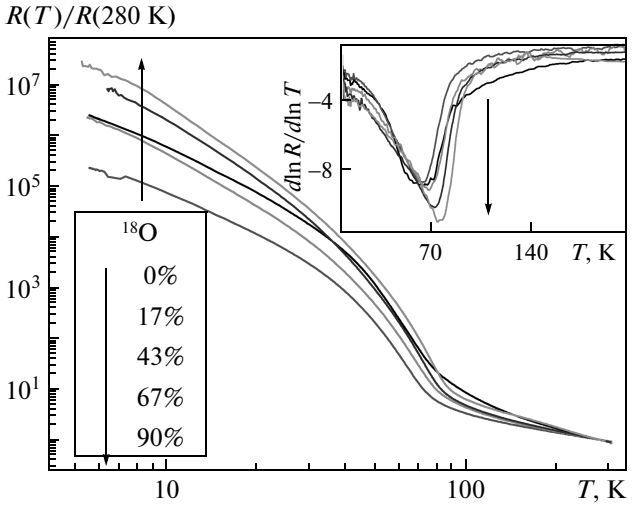

Fig. 9. Temperature dependence of the electrical resistivity for $(Pr_{1-y}Eu_y)_{0.7}Ca_{0.3}CoO_3$ with $y = 0.16$. The inset illustrates the behavior of the logarithmic derivative of $R(T)$

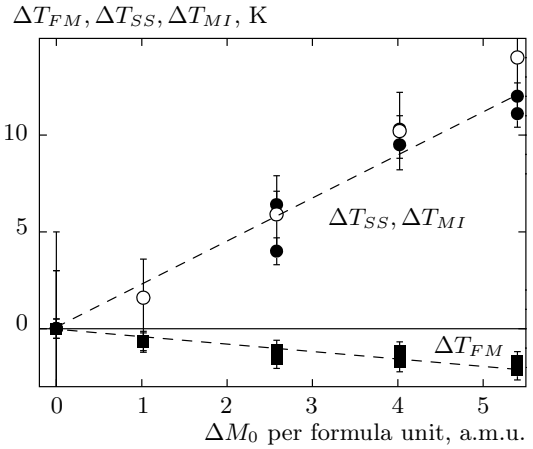

Fig. 10. Isotopic shift of the characteristic temperatures of the spin-state T_{SS}, metal–insulator T_{MI}, and ferromagnetic T_{FM} transitions for the sample with $y = 0.16$. The values of T_{SS} and T_{FM} were determined both on cooling and on heating the samples (two closed circles or squares at each isotope content). Open circles correspond to T_{MI}

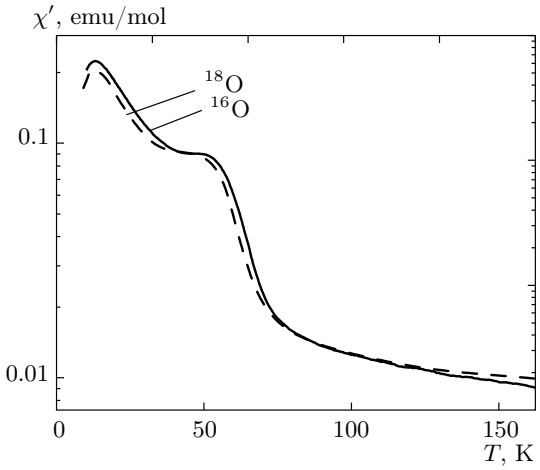

Fig. 11. Temperature dependence of the magnetic susceptibility for $(Pr_{1-y}Eu_y)_{0.7}Ca_{0.3}CoO_3$ with $y = 0.1$

in the paramagnetic range; this means that the absorption related to the itinerant charge carriers is very small and does not produce a significant effect on χ' and hence on the values of θ.

For the sample with $y = 0.16$ as well as for samples with $y = 0.14$, 0.2, we have found that the resistivity increases as the temperature decreases (by 5–7 orders of magnitude), with the MI transition in the vicinity of 70 K (Fig. 9). Both the resistivity and magnetic susceptibility data clearly indicate that this sample is in the phase-separation range. The temperatures of MI and SS transitions increase with the average oxygen mass (see the inset in Fig. 9). In the sample with $y = 0.16$, we see the same general tendency, namely, the increase in T_{SS} and the decrease in T_{FM} as the average oxygen isotope mass increases. Here, the values of the isotope constant are $\alpha_{SS,MI} = -(1.7 \pm 0.06)$ and $\alpha_{FM} = (0.34 \pm 0.1)$; the isotope shifts of the characteristic transition temperatures are illustrated in Fig. 10.

3. Finally, the samples with $y < y_{cr}$ (the Eu content $y = 0.10$) fall into the range of "nearly metallic" ferromagnets. In Ref. [17], it was shown that at $T < T_{FM}$, the compositions with a low Eu content correspond to the domains of the metallic ferromagnetic phase embedded in a weakly magnetic nonconducting matrix.

According to the temperature dependence $\chi'(T)$ plotted in Fig. 11, the magnetization steeply increases on cooling at about 60–70 K (i. e., the ferromagnetic phase arises). With the increase in the average oxygen mass, the value of $\chi'(T)$ decreases at low temperatures. Here, we have $T_{FM}(^{18}O) < T_{FM}(^{16}O)$ and the maximum isotope shift of T_{FM} does not exceed 2–3 K.

The electrical resistivity for these samples ($y = 0.10$) increases at low temperatures, even when the ferromagnetic phase arises. This behavior is quite similar to that observed in the samples with $y = 0.14$ and $y = 0.16$ (see Fig. 5). We note that the electrical resistance in the samples with ^{18}O is higher than in those with ^{16}O. However, with the decrease in the Eu con-

tent to $y = 0.10$, the MI peculiarity in the resistance is suppressed. Such behavior of $R(T)$ for samples with $y = 0.10$ can be compared with that for $y = 0.14$ samples (see Fig. 5 and the inset of that figure). The resistivity for samples with $y = 0.10$ corresponds to a more smooth curve than for samples with $y = 0.14$, although the regular course of the temperature dependence remains nearly unchanged. Thus, the samples with $y = 0.10$ do not become truly metallic, but their behavior differs from the behavior of the samples with $y = 0.14$ (they do not exhibit indications of an SST). Therefore, we argue that in the phase diagram, the composition with $y = 0.10$ lies outside the crossover region, on the left-hand side of it. The isotope constant is $\alpha_{FM} = (0.23 \pm 0.1)$.

We note here that for such a complicated system, there is no genuinely accurate method for determining thermodynamic values of the transition temperatures T_{SS} and, especially, T_{FM}. Probably, the closest to the actual value is the onset temperature of the transition (T^*). The value of T^* can be determined by different methods, but as we have already mentioned in Sec. 2, the isotope shift of the transition temperature is nearly insensitive to the definition of T^*. Therefore, in Figs. 3, 6, and 10, we show only the isotope shifts of the transition temperatures and not the temperatures themselves.

4. DISCUSSION OF EXPERIMENTAL RESULTS

The obtained data for the temperatures of the phase transitions can be represented in the form of a phase diagram (Fig. 12). It illustrates that as the Eu content increases, the system transforms from the nearly metallic ferromagnet to the LS insulating state, undergoing LS → IS spin-state transitions[1)]. Between these states, we have a broad crossover region corresponding to phase separation. Indeed, the simultaneous observation of both T_{FM} and T_{SS} in the samples with the Eu content $y = 0.14$, 0.16 is a clear evidence of the phase separation in the system.

These samples also provide a spectacular illustration of the effect related to the variable content of ^{18}O. In particular, for the samples with $y = 0.16$, the temperature dependence of the magnetic susceptibility (Fig. 4) exhibits a pronounced feature corresponding to

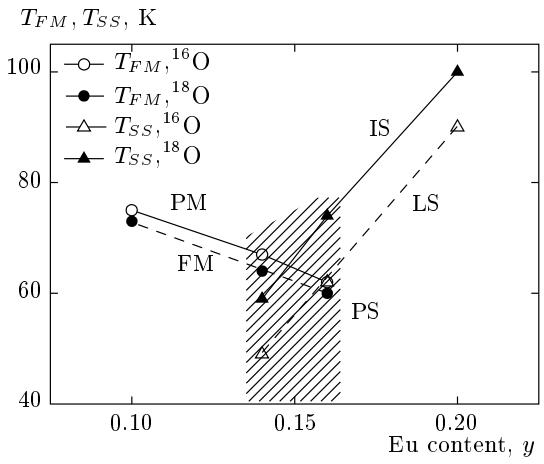

Fig. 12. Phase diagram of the $(Pr_{1-y}Eu_y)_{0.7}Ca_{0.3}CoO_3$ compound with ^{16}O and 90 % ^{18}O. PM, FM, IS, and LS respectively stand for the paramagnetic, ferromagnetic, intermediate-spin, and low-spin state. The hatched area corresponds to the phase-separated state (PS)

the SST at high values of the ^{18}O content. With decreasing the ^{18}O content, this feature becomes weaker and disappears below 17 % of ^{18}O. Hence, we see that the change in the average oxygen mass can drastically affect the phase composition of the cobaltite samples.

The oxygen isotope substitution ^{16}O → ^{18}O shifts the phase equilibrium toward the insulating state. For the heavier isotope, the SST temperature T_{SS} increases, while the ferromagnetic transition temperature T_{FM} decreases. Varying the average oxygen mass is a unique tool for investigating special properties of phase separation in cobaltites near the crossover between the FM and LS phases. We also see that the effect of increasing the ^{18}O content on the system is similar to that of increasing the Eu content.

We emphasize that the general structure of the phase diagram shown in Fig. 12 is similar to that reported in Ref. [17]. The partial oxygen isotope substitution allows a much more detailed study of the evolution of the state of doped perovskite cobaltites in the most interesting region corresponding to phase separation. This is exactly the main objective of our work, which could not be significantly affected by the difference in the composition of two sets of samples.

The analysis of these results for different chemical and isotope compositions demonstrates that the effect of the increase in the Eu content y and of the average oxygen mass are qualitatively similar. We can rescale the dependence of the transition temperature on both parameters using the combined variable $y + 0.015x$ for

[1)] As follows e. g. from the results of Ref. [16], the magnetic states of Co ions generated by doping are most probably IS states. For the following treatment, however, it is not critical whether we deal with the IS or HS states.

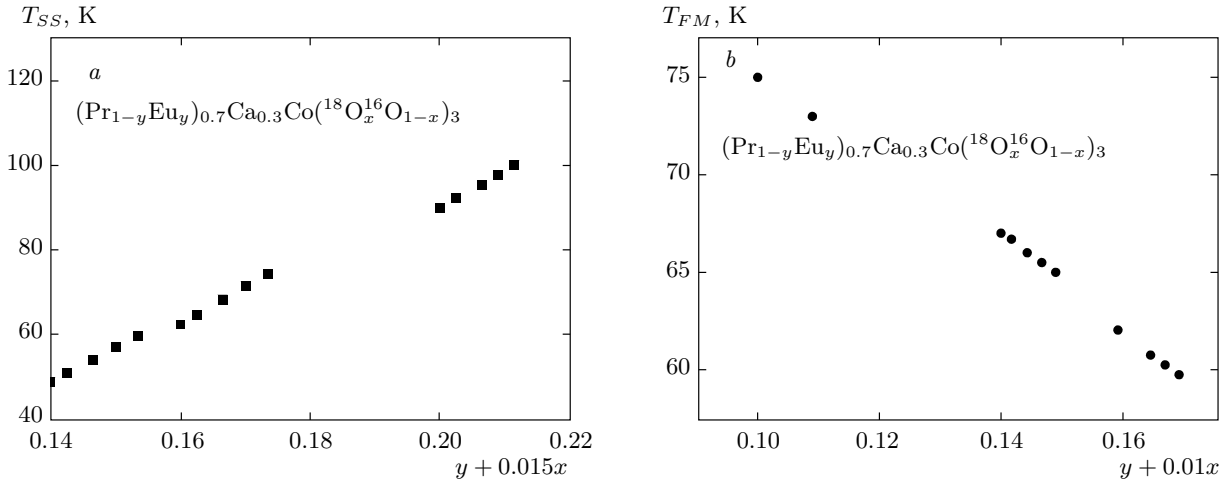

Fig. 13. Plots illustrating the combined effect of Eu and ^{18}O doping on the SST temperature of T_{SS} and on the ferromagnetic transition temperature T_{FM}. Note the difference of the temperature scales in panels (a) and (b)

T_{SS} or $y + 0.01x$ for T_{FM}, where x is the relative content of ^{18}O, as shown in Fig. 13. The temperatures of both the SS and FM transitions depend almost linearly on this combined variable. We see that the change in Eu content by 1 % is equivalent to the change in the isotope content by 70–100 %. This is actually the most important result of the present study. The theoretical analysis of these results is given in the next sections.

5. CALCULATION DETAILS

To explain the composition and isotope dependence of the properties of our system (see Fig. 12), especially the similar dependence of the SST temperature and the FM transition temperature illustrated in Fig. 13, we propose a realistic model (Section 7) based predominantly on the change of the electron bandwidth with the chemical and isotope composition. Some input, as well as the estimates of relevant parameters are taken from the *ab initio* band-structure calculations for the limiting "pure" compositions corresponding to $y = 0$ ($PrCoO_3$) and $y = 1$ ($EuCoO_3$).

The crystal structure of $PrCoO_3$ obtained in Ref. [20] for $T = 300$ K was used in those calculations. For $EuCoO_3$, the lattice parameters were taken from Ref. [21]. The exact atomic positions for $EuCoO_3$ are unknown, and we therefore used the same positions as for $PrCoO_3$ (with the correct unit cell volume for $EuCoO_3$). The splitting between different one-electron energy levels Δ_{CF} was calculated within the local density approximation (LDA) in the framework of the method of linear muffin-tin orbitals (LMTO) [22]. Partially filled but physically unimportant $4f$ states of the Eu and Pr were treated as frozen [23].

The Brillouin-zone (BZ) integration in the course of self-consistency iterations was performed over a mesh of 144 **k**-points in the irreducible part of the BZ.

6. DOPING DEPENDENCE: LDA RESULTS

There are different ways to estimate the SST temperature with the use of the band-structure calculation. The most direct way is to calculate the total energies of different spin states [24, 25]. However, in the case of a doped system, this would require very large supercells. Moreover, currently, we have no single commonly accepted model that can explain all experimental facts. Various combinations of a static or dynamic order of the different spin states are discussed in the literature [23, 26–29]. This is the reason why we chose an alternative approach.

The energy of any of the spin states depends on two important parameters: the single-electron energy difference Δ_{CFS} between the highest t_{2g} and the lowest e_g levels, and the intra-atomic Hund's rule exchange coupling J_H. The Hund's rule energy J_H is an atomic characteristic and does not change appreciably either with the Eu doping or with the isotope substitution. Hence, to investigate the dependence of the SST temperature on the doping or isotope substitution in the first approximation, we can focus on the study of the single parameter, Δ_{CFS}. If Δ_{CFS} is large enough ($\Delta_{CFS} > 2J_H$), it is energetically favorable to localize all electrons in the low-lying t_{2g} subshell of Co^{3+},

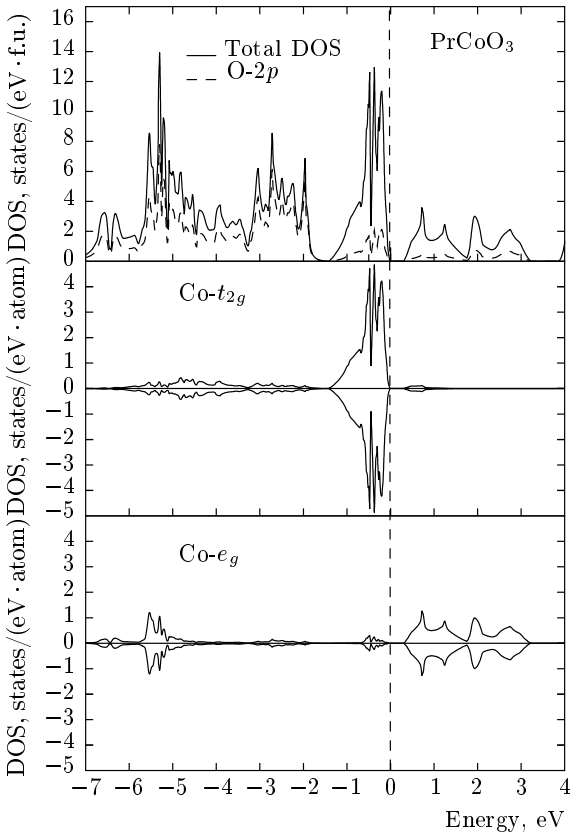

Fig. 14. The total and partial densities of states (DOS) for $PrCoO_3$. The Fermi energy corresponds to zero

i. e., the system is in the LS state. With a decrease in the crystal-field splitting, some electrons can be transferred to the e_g subshell, which allows the system to gain the exchange energy, because there are more electrons with the same spin. As we show below, both the isotope substitution and the doping can be related to the crystal-field splitting.

To estimate Δ_{CFS}, we used the Wannier function projection procedure proposed in Ref. [30], which allows projecting the full-orbital band Hamiltonian onto the subspace of a few states (five d states of Co). With the Fourier transformation, we obtain the Hamiltonian in real space, from which the splitting between t_{2g} and e_g can be easily calculated. For $PrCoO_3$, we obtain $\Delta_{CFS} = 2.07$ eV.

The total and partial densities of states (DOS) obtained for $PrCoO_3$ in the LDA calculations are presented in Fig. 14. In the octahedral symmetry, the $3d$ states of Co are split into t_{2g} and e_g subbands. In the LDA, the valence band is mostly formed by the Co-t_{2g} states, while the conduction band is determined by the Co-e_g states. The O-$2p$ band is located in the energy range from -7 to -1.5 eV.

The DOS for $EuCoO_3$ is qualitatively very similar and the corresponding calculations of Δ_{CFS} result in the value of 2.14 eV. The increase in the t_{2g}–e_g excitation energy in passing from $PrCoO_3$ to $EuCoO_3$ is caused by two factors. The first is the lanthanide contraction: the substitution of the large Pr^{3+} by smaller Eu^{3+} ions leads to some decrease in the Co–O distance and to the corresponding increase in the p–d hybridization, which leads to an increase in the difference between the centers of the t_{2g} and e_g bands. The second effect is related to the decrease in the effective widths of t_{2g} and e_g energy bands with the corresponding increase in the energy gap between them. This narrowing of energy bands in passing from $PrCoO_3$ to $EuCoO_3$ is also related, in effect, to the lanthanide contraction, which is the cause of the tilting of CoO_6 octahedra to increase and the Co–O–Co angle and the corresponding bandwidth to decrease in passing from $PrCoO_3$ to $EuCoO_3$. Both these effects eventually lead to the increase in Δ_{CFS} with the Eu content, which leads to the enhanced stabilization of the LS state of Co^{3+} (see a more detailed discussion of these effects in Sec. 7).

This change of the crystal-field splitting (CFS) results in the modification of the SST temperature, since this transition is due to the competition of the Hund's rule exchange coupling J_H and the CFS [23].

It was found in Refs. [17] and [31] (also see Fig. 12) that the change of the Eu content y in $(Pr_{1-y}Eu_y)_{0.7}Ca_{0.3}CoO_3$ by 0.02 leads to the change of the SST temperature by about 14 K. In the first approximation, it is possible to neglect the presence of Ca and interpolate the change of the CFS for the complex system like $(Pr_{1-y}Eu_y)_{0.7}Ca_{0.3}CoO_3$ using the CFS values for $y = 1$ ($PrCoO_3$) and $y = 0$ ($EuCoO_3$). Indeed, the substitution of Ca for Eu^{3+}/Pr^{3+} gives rise to ligand holes, which manifest themselves mainly in the rigid shift of the O-$2p$ band upward, resulting in a slight increase of the CFS. Such a linear interpolation predicts the change of the SST temperature by 16 K if y changes by 0.02, which is in excellent agreement with the experiment.

7. ISOTOPE SUBSTITUTION: MODEL RESULTS

The isotope substitution does not change the chemical properties of ions such as the oxidation numbers or bonding energies. However, it affects the crystal lattice via a modification of the phonon spectra. Below, following the approach in Ref. [32], we demonstrate the

effect of this modification on the electronic and magnetic properties and hence on the SST.

In the tight-binding model, the band spectrum of a solid is determined by the on-site ionic energy levels ε_i^{nlm} and the hopping matrix elements between different sites $t_{ij}^{ll',mm'}$. The ionic energies ε_i^{nlm} are obviously independent of the mass of the ions, being determined by the quantum numbers and the intra-atomic Coulomb and exchange interactions. The hopping parameters depend on the type of the orbitals (s, p, d, f), the bonding type (π, σ, δ), and the distance between ions u. According to the famous Harrison parameterization [33, 34] in the absence of lattice vibrations, the hopping integrals, e. g., between p orbitals of the oxygen and transition metal d-orbitals equal to

$$t_{pd} = C_{pdm}/u^4, \tag{1}$$

where coefficients C_{pdm} depend on the bonding type and can be different for different metals and ligands [33, 35].

The static version of Eq. (1) can be generalized by taking the presence of lattice vibrations, i. e., phonons into account, which depend on the ion masses. The mean pd hopping matrix element can be calculated as

$$\langle t_{pd}\rangle = \frac{1}{2v}\int\limits_{u_0-v}^{u_0+v}\frac{C_{pdm}}{u^4}\,du = \\ = \frac{C_{pdm}}{6v}\left(\frac{1}{(u_0-v)^3}-\frac{1}{(u_0+v)^3}\right), \tag{2}$$

where $v = \sqrt{\langle \delta u^2\rangle}$ is the mean square displacement from the equilibrium position u_0 due to phonons. Since $v/u_0 \ll 1$, we can simplify the last equation by expanding it in a series to the 4th order

$$\langle t_{pd}\rangle = \frac{C_{pdm}}{u_0^4}\left(1+\frac{10}{3}\left(\frac{v}{u_0}\right)^2\right)+O\left(\left(\frac{v}{u_0}\right)^4\right). \tag{3}$$

In the static limit $v \to 0$, the last formula coincides with Eq. (1).

In the Debye model at zero temperature, the mean-square displacement is written as [36]

$$v^2 = \langle \delta u^2\rangle = \frac{9\hbar^2}{4k_B\theta_D}\,\frac{1}{m}, \tag{4}$$

where m is the mass of vibrating ions and θ_D is the Debye temperature. Due to different masses, the mean-square displacements in the compounds enriched by ^{16}O or ^{18}O are different. The Debye temperature for a very similar system, $LaCoO_3$, was found to be about 600 K [37]. We can use this value to estimate v in $(Pr_{1-y}Eu_y)_{0.7}Ca_{0.3}CoO_3$. Then, the mean-square displacement is $v_{18} = 0.100$ Å for ^{18}O and $v_{16} = 0.107$ Å for ^{16}O. According to Eq. (3), this leads to a decrease in the effective bandwidth in passing from ^{16}O to ^{18}O. A qualitative explanation of this effect is presented in Fig. 15*a*. For strong electron–phonon coupling, the same effect could be attributed to the polaron-band narrowing depending on the isotope mass.

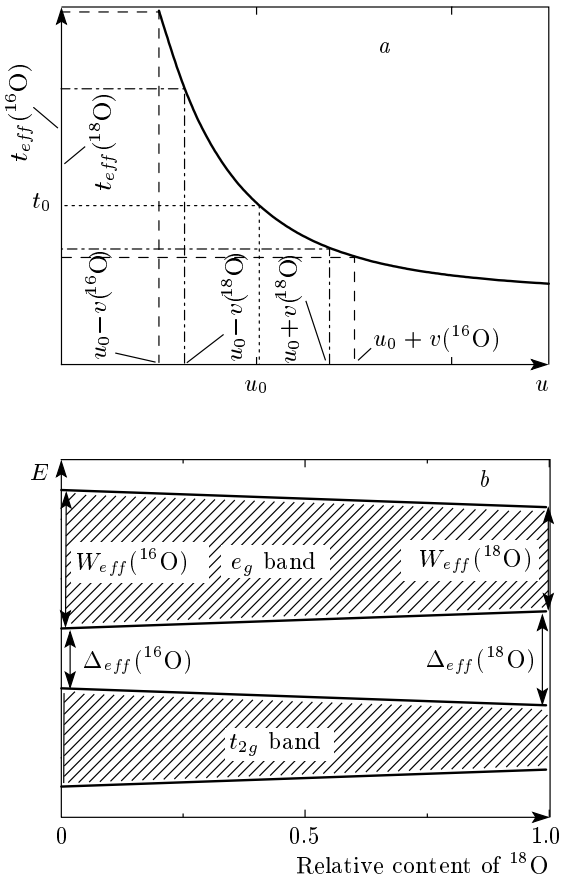

Fig. 15. Schematic illustration of the effects of oxygen isotope substitution (*a*) on the effective hopping integral t_{eff} and (*b*) on the effective gap Δ_{eff} between the e_g and t_{2g} bands and on the effective width W_{eff} of the e_g band. The solid curve in panel (*a*) depicts the hopping integral t as function of the inter-ion distance u according to Eq. (1). The effective hopping integrals t_{eff} are determined by averaging $t(u)$ over the interval given by the mean-square displacement v of ions due to lattice vibrations (4) (crudely, $t_{eff} = 1/2[t(u_0+v)+t(u_0-v)]$ for each isotope). We see that $t_{eff}(^{16}O) > t_{eff}(^{18}O)$. As a result, $\Delta_{eff}(^{18}O) > \Delta_{eff}(^{16}O)$, and hence $T_{SS}(^{18}O) > T_{SS}(^{16}O)$. At the same time, $W_{eff}(^{18}O) < W_{eff}(^{16}O)$, and hence $T_{FM}(^{18}O) < T_{FM}(^{18}O)$

The SST temperature depends on the energy difference between the t_{2g} and e_g subbands, which is defined by the widths of corresponding bands and the positions of their centers. We start with the study of the bandwidth dependence on the ligand ion mass (see the schematic illustration in Fig. 15*b*).

To calculate the change in the bandwidth caused by the $^{16}O \to {}^{18}O$ substitution, we need to know the hopping integrals, which depend on two unknown parameters C_{pdm} and u_0. The C_{pdm} coefficients can in principle be evaluated as is prescribed, for instance, in Ref. [33]. However, for a better precision, we calculated the C_{pdm} parameters from the LDA t_{2g} and e_g bandwidths in pure $PrCoO_3$. The equilibrium Co–O distance u_0 in its turn can be evaluated from the actual crystal structure data for $EuCoO_3$ and $PrCoO_3$.

Finally, performing all these calculations, we obtain that the t_{2g} bandwidth decreases by 22 K when ^{16}O is replaced by ^{18}O. The decrease in the e_g bandwidth is two times larger and equals 44 K. In effect, the minimum energy of the $t_{2g} \to e_g$ transition increases by 33 K. Hence, the SST temperature due to the change of the bandwidth must increase similarly in passing from ^{16}O to ^{18}O in qualitative accordance with the experiment (we even overestimate the actually observed changes; see Fig. 12).

We consider the second mechanism that affects the SST and is related to the dependence of changes in the centers of gravity of the corresponding bands (i. e., CFS) with the isotope substitution. It turns out that this effect counteracts the first one (change of the effective t_{2g} and e_g bandwidths), but this second effect is much smaller numerically (see below). Generally speaking, there are two main contributions to the CFS Δ_{CFS}. One comes from the Coulomb interaction of the $3d$ electrons with the negatively charged ligands, and the other is due to the hybridization between d orbitals of metal ions and p orbitals of the ligands [38, 39]. For most oxides of $3d$ transition metals, both terms act "in the same direction", resulting in the same sequence of levels [40]. That is why the approaches so crude as the atomic sphere approximation (ASA) [41] often used in *ab initio* calculations provide quite precise band structure in most cases. The effect of the Coulomb term can be omitted or effectively incorporated into the kinetic energy contribution. Below, we follow the same strategy by considering the kinetic energy only, keeping in the mind that the Coulomb contribution can be taken into account by the parameter renormalization.

In the second order of the perturbation theory, the CFS between t_{2g} and e_g subbands is written as

$$\Delta_{CFS} = \frac{t_{pd\sigma}^2 - t_{pd\pi}^2}{\Delta_{CT}}, \tag{5}$$

where Δ_{CT} is the charge-transfer energy (which corresponds to the $d^n p^6 \to d^{n+1} p^5$ transition) and $t_{pd\sigma}$ and $t_{pd\pi}$ are the hopping matrix elements for different types of bonds.

Because the average hopping $\langle t_{pd} \rangle$ decreases in passing from ^{16}O to ^{18}O according to Eqs. (3) and (4), the CFS should also decrease as follows from Eq. (5). As a result, this contribution should lead to the opposite tendency: a decrease in the SST temperature in going from ^{16}O to ^{18}O. However, this effect does not exceed a few kelvins at realistic values of the charge-transfer energy in cobaltites [42].

We also note that we here estimated the changes in the distance between the *edges* of t_{2g} and e_g subbands. However, at finite temperatures, we must have transitions not only between the band edge but also from one subband to another. Such a temperature-induced smearing could also somehow diminish our estimates of the isotope effect in SST.

In Fig. 13*b*, we see that the isotope effect for T_{FM}, being much weaker than for T_{SS}, is of the opposite sign. Nevertheless, there is the same similarity between the effects of the Eu content and the oxygen isotope substitution. This is in agreement with our expectations, because the ferromagnetism of the low-Eu doped samples with metallic clusters should be stabilized by the double-exchange mechanism, according to which T_{FM} is proportional to the effective bandwidth of itinerant electrons. This bandwidth decreases for the heavier isotope, and that is why T_{FM} decreases at the $^{16}O \to {}^{18}O$ substitution as well as at increasing the Eu content (see Fig. 13*b*). A schematic illustration of the mechanism underlying the oxygen isotope effect discussed above is given in Fig. 15.

8. CONCLUSIONS

Experimental studies carried out for $(Pr_{1-y}Eu_y)_{0.7}Ca_{0.3}CoO_3$ cobaltites with the varying isotope substitution of ^{16}O by ^{18}O demonstrated that there exists a strong similarity in the changes caused by the chemical composition (increasing the Eu content) and those arising from the oxygen isotope substitution. The chemical composition $y \sim 0.1$–0.2 was chosen because a crossover between the ferromagnetic near-metallic state with magnetic Co ions to the nonmagnetic insulator with the low-spin Co^{3+} ($t_{2g}^6 e_g^0$, $S = 0$) occurs in this range, see Fig. 12.

The main experimental conclusion presented in Fig. 13 is that the behavior of this system can be rescaled. The dependence of the SST temperature and of the ferromagnetic transition temperature on the Eu content y and on the content x of the heavier isotope ^{18}O can be represented by the same almost linear plot as a function of the respective combined variables $y + 0.015x$ and $y + 0.01x$. This means, for example, that under the SST, the change of the Eu content y by 0.007 is equivalent to the substitution of 50 % of ^{16}O by ^{18}O. In addition, this clearly demonstrates that not only the average transition temperatures change with the doping and isotope substitution, but also the transition temperatures for each separate phase vary with the chemical and isotope composition.

Based on this similarity between the role of chemical and isotope composition for the SST and for the transition to the ferromagnetic state at a lower Eu content, we propose a theoretical explanation of the isotope effect in these transitions. We investigate the corresponding changes and estimate the relevant parameters using *ab initio* band structure calculations. These results together with an analytic model allow explaining the observed behavior. In particular, the isotope effect both in the spin-state and ferromagnetic transitions is interpreted in terms of the change in the corresponding widths of the d bands occurring due to the electron–phonon renormalization, which depends on the atomic masses of the respective isotopes.

All this demonstrates once again that the oxygen isotope substitution is a powerful tool for revealing salient features in the behavior of strongly correlated magnetic oxides.

Summarizing, we can say that using this approach, we established, first, that in the aforementioned crossover range, we can clearly distinguish two coexisting phases, a nearly insulating one exhibiting an SST and a nearly metallic "ferromagnetic" one, with different behaviors of the transition temperatures. Second, we have found that these transition temperatures depend almost linearly on the content of the heavy oxygen isotope, which is a nontrivial observation clearly demonstrating that the electronic structure can be effectively controlled by isotopes. Third, based on these observations and using the parameters deduced from our band-structure calculations, we put forward a simplified model capturing the main physics of the isotope effect in the systems with SSTs and quantitatively describing the experimental data.

This work is supported by the Russian Foundation for Basic Research (projects 10-02-00598-a, 10-02-00708-a, 11-02-91335-NNIO-a, and 13-02-00374), by the Ministry of Education and Science of Russia (grant MK-344320132) by the Ural Branch of Russian Academy of Sciences through the young-scientist program, by the German projects DFG GR 1484/2-1, FOR 1346, by Köln University via German Excellence Initiative, and by the European network SOPRANO.

REFERENCES

1. N. A. Babushkina, L. M. Belova, O. Yu. Gorbenko et al., Nature **391**, 159 (1998).
2. J. B. Goodenough and P. M. Raccah, J. Appl. Phys. **36**, 1031 (1965).
3. K. Asai, A. Yoneda, O. Yokokura et al., J. Phys. Soc. Jpn. **67**, 290 (1998).
4. T. Saitoh, T. Mizokawa, A. Fujimori et al., Phys. Rev. B **55**, 4257 (1997).
5. Y. Tokura, Y. Okimoto, S. Yamaguchi et al., Phys. Rev. B **58**, R1699 (1998).
6. M. A. Korotin, S. Y. Ezhov, I. V. Solovyev et al., Phys. Rev. B **54**, 5309 (1996).
7. K. Berggold, M. Kriener, P. Becker et al., Phys. Rev. B **78**, 134402 (2008).
8. N. B. Ivanova, S. G. Ovchinnikov, M. M. Korshunov et al., Usp. Fiz. Nauk. **179**, 837 (2009).
9. R. Ganguli, A. Maignan, C. Martin et al., J. Phys.: Condens. Matter **14**, 8595 (2002).
10. J. Wu and C. Leighton, Phys. Rev. B **67**, 174408 (2003).
11. D. Phelan, Despina Louca, and K. Kamazawa, Phys. Rev. Lett. **97**, 235501 (2006).
12. A. Podlesnyak, M. Russina, A. Furrer et al., Phys. Rev. Lett. **101**, 247603 (2008).
13. A. O. Sboychakov, K. I. Kugel, A. L. Rakhmanov, and D. I. Khomskii, Phys. Rev. B **80**, 024423 (2009).
14. J. Yu, Despina Louca, D. Phelan, K. Tomiyasu et al., Phys. Rev. B **80**, 052402 (2009).
15. S. El-Khatib, Shameek Bose, C. He et al., Phys. Rev. B **82**, 100411 (2010).
16. A. Podlesnyak, G. Ehlers, and M. Frontzek, Phys. Rev. B **83**, 134430 (2011).
17. A. V. Kalinov, O. Yu. Gorbenko, A. N. Taldenkov et al., Phys. Rev. B **81**, 134427 (2010).

18. N. A. Babushkina, A. N. Taldenkov, L. M. Belova et al., Phys. Rev. B **62**, R6081 (2000).

19. A. M. Balagurov, V. Yu. Pomjakushin, D. V. Sheptyakov et al., Mater. Sci. Eng. B **116**, 64 (2005).

20. K. Knížek, J. Hejtmánek, Z. Jirák et al., Phys. Rev. B **79**, 134103 (2009).

21. J. Baier, S. Jodlauk, M. Kriener, A. Reichl et al., Phys. Rev. B **71**, 014443 (2005).

22. O. K. Andersen and O. Jepsen, Phys. Rev. Lett. **53**, 2571 (1984).

23. I. A. Nekrasov, S. V. Streltsov, M. A. Korotin, and V. I. Anisimov, Phys. Rev. B **68**, 235113 (2003).

24. S. V. Streltsov and N. A. Skorikov, Phys. Rev. B **83**, 214407 (2011).

25. M. A. Korotin, S. Yu. Ezhov, I. V. Solovyev et al., Phys. Rev. B **54**, 5309 (1996).

26. K. Knížek, Z. Jirák, J. Hejtmánek et al., Phys. Rev. B **79**, 014430 (2009).

27. Y. Ren, J.-Q. Yan, J.-S. Zhou et al., Phys. Rev. B **84**, 214409 (2011).

28. M. W. Haverkort, Z. Hu, J. C. Cezar et al., Phys. Rev. Lett. **97**, 176405 (2006).

29. K. V. Lamonova, E. S. Zhitlukhina, R. Yu. Babkin et al., J. Phys. Chem. A **115**, 13596 (2011).

30. S. V. Streltsov, A. S. Mylnikova, A. O. Shorikov et al., Phys. Rev. B **71**, 245114 (2005).

31. N. Babushkina, A. Taldenkov, A. Kalinov et al., Zh. Eksp. Teor. Fiz. **138**, 215 (2010).

32. N. A. Babushkina, L. M. Belova, V. I. Ozhogin et al., J. Appl. Phys. **83**, 7369 (1998).

33. W. Harrison, *Elementary Electronic Structure*, World Scientific, Singapore (1999).

34. O. Andersen and O. K. Jepsen, Physica B **91**, 317 (1977).

35. J. C. Slater and G. F. Koster, Phys. Rev. **94**, 1498 (1954).

36. J. Reissland, *The Physics of Phonons*, Wiley, New York (1973).

37. S. Stølen, F. Grønvold, H. Brinks et al., Phys. Rev. B **55**, 14103 (1997).

38. C. Ballhausen, *Introduction to Ligand Field Theory*, McGraw-Hill, New York (1962).

39. H. Sugano, S. Tanabe, and Y. Kamimura, *Multiplets of Transition-Metal Ions in Crystals*, Acad. Press, New York (1970).

40. A. Ushakov, S. V. Streltsov, and D. I. Khomskii, J. Phys.: Condens. Matter **23**, 445601 (2011).

41. H. Skiver, *The LMTO Method*, Springer-Verlag, Berlin (1984).

42. A. Chainani, M. Mathew, and D. D. Sarma, Phys. Rev. B **46**, 9976 (1992).